Suppression of ionization and atomic electron localization by short intense laser pulses

Q. Su and J. H. Eberly

Department of Physics and Astronomy, University of Rochester, Rochester, New York 14627

(Received 2 July 1990)

Ionization suppression and electron localization have been observed in numerical modeling of two-photon ionization by very intense short-wavelength laser fields. In this paper we present similar results for one-photon ionization. We find that a one-dimensional atom follows one of three distinct routes to ionization depending whether the field is weak, strong, or superstrong. The first route can be described by perturbation theory. The second route is characterized by very rapid depletion of the bound-state population, leading to 100% ionization. The third route features incomplete ionization and electron localization. The behavior of the atom in both strong and superstrong fields is strongly correlated with the deformation of the atomic binding potential associated with the Kramers-Henneberger frame transformation.

I. INTRODUCTION

Fermi's golden rule is generally satisfactory for calculating one-photon ionization rates. Based on perturbation theory, it works well in weak radiation fields. Today's laser technology, however, allows very strong fields to be generated in the laboratory. These strong field intensities are in the range 0.01–100 atomic units (1 a.u. $\sim 3.5 \times 10^{16}$ W/cm^2). The nature of the ionization process in such strong fields is still an open question. We try to address this question in this paper by studying numerically a model atom interacting with a short very intense laser pulse.[1]

The main difficulty in theoretical studies of strong-field ionization comes from the dipole interaction term in the Hamiltonian. To obtain a fundamental understanding of ionization one should solve the Schrödinger equation and obtain the time-dependent electron wave function. In our study we consider the equation (in atomic units)

$$i\frac{\partial}{\partial t}\Psi(x,t) = \left[-\frac{1}{2}\frac{\partial^2}{\partial x^2} + V(x) + x\,\mathcal{E}(t)\sin\omega t \right]\Psi(x,t)$$

(1)

which is the one-dimensional version of the "true" one-electron Schrödinger equation. The dipole term on the right-hand side is unbounded in x and is of course very large for a strong electric field. A perturbative treatment of this term is now recognized to be unsatisfactory for $\mathcal{E} > 0.10$. It is also generally agreed that a nonperturbative treatment based on Volkov electron states can grossly misrepresent the effects of $V(x)$.

Under such circumstances, we find it very convenient to consider the point of view taken by Henneberger[2] in 1968 and later by Gersten and Mittleman,[3] and Gavrila and collaborators.[4] Henneberger first attempted to treat the ionization of hydrogen in very strong fields by transforming to the frame of a free electron. To get this frame, consider the unitary transformation:

$$\Psi(x,t) = e^{iA(t)x/c}\exp\left[-i\int d\tau\left[\frac{A^2}{2c^2}\right]\right]$$
$$\times e^{-i\alpha p}\Psi_{KH}(x,t) ,$$

(2)

where A denotes the vector potential

$$A(t) = -c\int_0^t d\tau\,\mathcal{E}(\tau)\sin\omega\tau ,$$

(3)

$p = -i\partial/\partial x$ is the momentum operator, c is the speed of light, and α satisfies

$$\ddot{\alpha} = \frac{\dot{A}}{c} = -\mathcal{E}(t)\sin\omega t$$

(4)

which describes the motion of a free electron in the field. The transformation shown in Eq. (2) removes the dipole interaction term and transforms the Schrödinger equation to

$$i\frac{\partial}{\partial t}\Psi_{KH}(x,t) = \left[-\frac{1}{2}\frac{\partial^2}{\partial x^2} + V(x+\alpha) \right]\Psi_{KH}(x,t) .$$

(5)

(This transformation was employed earlier by Kramers for other purposes,[5] and we will use the term Kramers-Henneberger or KH transformation.)

Equation (5) has no known solution for any nontrivial potential $V(x)$ due to the implicit time dependent of α. But for a short-wavelength (high-frequency) laser, one can expect that the cycle-averaged binding potential will contribute most of the physics. Without the external laser field, the attraction by the nucleus produces a potential well centered at the origin. In a strong field, the time average of $V(x+\alpha)$ is a double well with two minima separated by twice the classical excursion distance $\alpha_0 = \mathcal{E}/\omega^2$. In this picture, the atomic Hamiltonian is time independent. Consequently, all of its eigenstates are stable and ionization is impossible. Gavrila and co-workers[4] have emphasized that the two minima give a two-peaked character (so-called "dichotomy") to the electron's eigenfunctions in this average potential.

There is no proof that the time-averaged KH potential

is suitable for the analysis of a real ionization process, particularly if the laser field is pulsed on and off. However our atomic wave function calculations suggest that the basis set associated with this deformed potential is quite sufficient for describing the effect of short-wavelength lasers in surprising detail. One advantage of using this framework can be seen from the fact that the potential-free solution of Eq. (5) is trivially obtained, and the transformation (2) then gives (equally trivially)

$$\Psi(x,t) = e^{iAx/c}\exp\left[-i\int d\tau\left[\frac{A^2}{2c^2}\right]\right]$$
$$\times e^{-ik^2t/2}e^{ik(x-\alpha)} , \tag{6}$$

which is a so-called Volkov state,[6] the state of a free electron dressed by the electric field. In a Volkov state the threshold upshift is fully accounted for. We will see later that for $V \neq 0$ the bound states in the average KH frame also reflect the existence of level shifts in the field. In a sufficiently weak field these shifts are the same as the lowest-order ac Stark shifts.

In Sec. II we discuss the properties of the average potential in the KH frame. These properties include the potential well deformation, shifted eigenenergies, and the condition for a double well to emerge from the original single-well structure. In Sec. III we report the ionization probabilities for various field intensities. We compare several weak-field ionization rates with the Fermi golden rule predictions. In Sec. IV we present plots of the electron's spatial probability density distribution and distinguish three routes to ionization: perturbative ionization, saturation of ionization, and suppression of ionization. In Sec. V we display the electron's above-threshold energy distributions (ATI spectra) for various field strengths. We confirm the correlation between the main ATI peak positions and the shifted energy levels introduced in Sec. II. Section VI summarizes our work.

II. FIELD-DEFORMED POTENTIAL AND ITS EIGENVALUES

As mentioned in the Introduction, the Schrödinger equation in the KH frame takes a relatively simple form. In this frame, the potential not only describes the electron-core attraction but it also includes the effect of electron oscillations in the field. Notice that the time dependence brought in by α is periodic with frequency ω, so it makes sense to expand the potential function into a Fourier series

$$V(x+\alpha(t)) = \sum_{m=-\infty}^{\infty} V_m(x;\alpha_0)e^{im\omega t} . \tag{7}$$

It was already emphasized by many researchers[2–4] that for high-frequency lasers, $V_0(x;\alpha_0)$ plays the most critical role. The argument is based on the fact that all higher-order Fourier components are effectively averaged out on the physical time scale. We will call $V_0(x;\alpha_0)$ the field-deformed potential. As will be shown, $V_0(x;\alpha_0)$ is also a bounded potential and has a corresponding set of eigenlevels.

Up to now we have not mentioned any specific form of

potential function. In previous computations[1,7–9] we have used the long-range potential $V(x) = -1/\sqrt{1+x^2}$. The field-deformed potential for this $V(x)$ is

$$V_0(x;\alpha_0) = -\frac{1}{2\pi}\int_{-\pi}^{\pi} d\varphi \frac{1}{[1+(x+\alpha_0\sin\varphi)^2]^{1/2}} , \tag{8}$$

where $\alpha_0 = \mathcal{E}/\omega^2$ and $\varphi = \omega t$. In Fig. 1(a) we have plotted $V_0(x;\alpha_0)$ vs x for $\alpha_0 = 0$ and 7.8 corresponding to $\mathcal{E} = 0$ and 5 for our one-photon ionization case ($\omega = 0.8$). The graph shows that a much shallower potential is formed for $\mathcal{E} = 5$. The zero-field single-well potential located at the center has deformed to a double-well structure symmetric about the origin. The dips of the double well are about α_0 away from the center. In Fig. 1(b) we have plotted the bound-state energies in the field-deformed potential for electric field strengths up to $\mathcal{E} = 15$. Naturally, as the potential gets shallower the ground level gets gradually lifted up. It is interesting to see that the first excited level becomes nearly degenerate with the ground level as $\mathcal{E}$ gets larger. The wave functions for these levels take their maximum values in the region of the two dips. They are symmetric and antisymmetric functions with very close eigenvalues for large enough $\mathcal{E}$.

Since the double-well structure is very important in the following discussions, we shall make a rough estimate as to when it emerges. The criterion we use here is convexity of the potential at the origin:
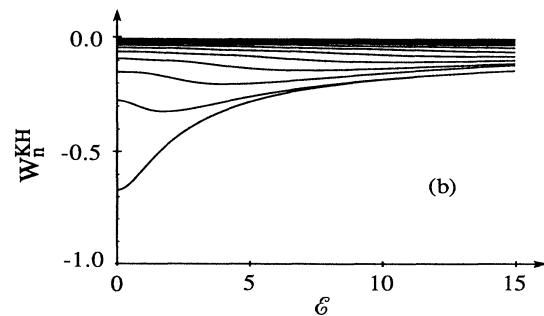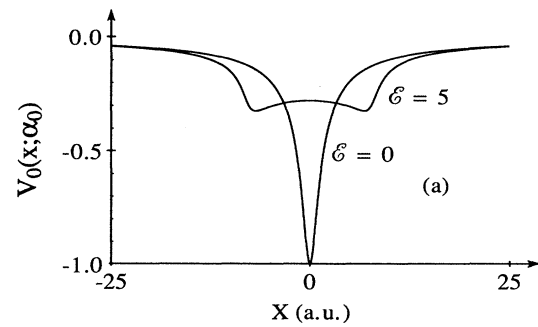

FIG. 1. (a) Average atomic binding potential in the KH frame for $\mathcal{E} = 0$ and 5. (b) Energy levels in the average KH frame for values of $\mathcal{E}$ up to $\mathcal{E} = 15$.

$$\frac{\partial^2}{\partial x^2} V_0 \Big|_{x=0} = \frac{2}{\pi} \int_0^{\pi/2} d\varphi \frac{1 - 2\alpha_0^2 \sin^2\varphi}{(1 + \alpha_0^2 \sin^2\varphi)^{5/2}} \leq 0 \ . \quad (9)$$

The second derivative equals zero for the critical value

$$(\alpha_0)_c \approx 2.18 \ . \quad (10)$$

For $\omega = 0.8$, the corresponding critical electric field strength is $\mathscr{E}_c = 1.74$ (corresponding in the intensity 10^{17} W/cm^2).

Our bare atom, characterized by the potential $V(x) = -1/\sqrt{1 + x^2}$, has the ground-state energy -0.67 a.u. However, simple scaling rules exist[10] by which this ground-state energy can be shifted at will, and ω and $\mathscr{E}_c$ both shifted the same time. For a lower ionization potential than 0.67 a.u., the critical field strength and intensity are also lower (see Ref. 10).

III. IONIZATION PROBABILITIES IN WEAK AND STRONG FIELDS

The time dependent ionization can be defined as

$$P(t) = \int dW |\langle W | \Psi(t) \rangle|^2 \quad (11a)$$

or

$$P(t) = 1 - \sum_n |\langle n | \Psi(t) \rangle|^2 \ . \quad (11b)$$

The integration in Eq. (11a) is carried over all the positive energy states of the field-free potential and the summation in Eq. (11b) is carried over all the bound states. The two definitions should give the same result for the ionization probability because the bound and the continuum states together form a complete set. We have checked for weak-field cases that the two definitions agree with each other to a high accuracy. For stronger fields, expression (11b) is easier to use because the number of bound states is fixed for the spatial size picked in the numerical computations. In either case it is clear that here we mean positive-energy probability when we say ionization probability.

In Fig. 2(a) we have plotted the ionization probabilities for $\mathscr{E} = 0.03 - 1$. We show the result for $\mathscr{E} = 5$ in Fig. 2(b) and for $\mathscr{E} = 15$ in Fig. 2(c). We can divide these ionization curves roughly into three different groups according to their intensities. The first group is defined by $\alpha_0 = \mathscr{E}/\omega^2 \ll (\alpha_0)_c$ where $(\alpha_0)_c$ is defined in Eq. (10). Intensities in this group are called weak and all cases with $\mathscr{E} \leq 0.10$ in Fig. 2(a) belong to this group. The second group is defined by $\alpha_0 \sim (\alpha_0)_c$. Intensities in this group are called strong. $\mathscr{E} = 0.5$ and 1 in Fig. 2(a) belong to this region. The third group is defined by $\alpha_0 > (\alpha_0)_c$. Intensities in this group are called superstrong. The cases with $\mathscr{E} = 5$ in Fig. 2(b) and $\mathscr{E} = 15$ in Fig. 2(c) belong to this region. We shall see that various ionization properties follow this intensity classification.

We see that the weak-field ionization probabilities for $\mathscr{E} = 0.03 - 0.10$ in Fig. 2(a) grow almost linearly in time after the pulse turn-on. (In all of the calculations shown we have used laser pulses with 50.25 cycle duration and 10.25 cycle smooth turn-on time.) The slopes of these curves correspond to the ionization rate. The slope for

the weakest field ($\mathscr{E} = 0.03$), for example, gives an ionization rate value of 1.31×10^{-4} a.u. An estimate based on the Fermi golden rule (FGR)

$$R_1 = 2\pi \left[\frac{\mathscr{E}}{2}\right]^2 \rho(W_f) |x_{i \to f}|^2 \ , \quad (12)$$

where $\mathscr{E} = 0.03$, $\rho(W_f) = \rho(0.130) = 1419.95/2$, and $|x_{i \to f}| = 0.011\,579$, gives $R_1 = 1.35 \times 10^{-4}$ a.u. The agreement between the numerical result and this estimate is within 3%. Rates for stronger fields naturally lead to
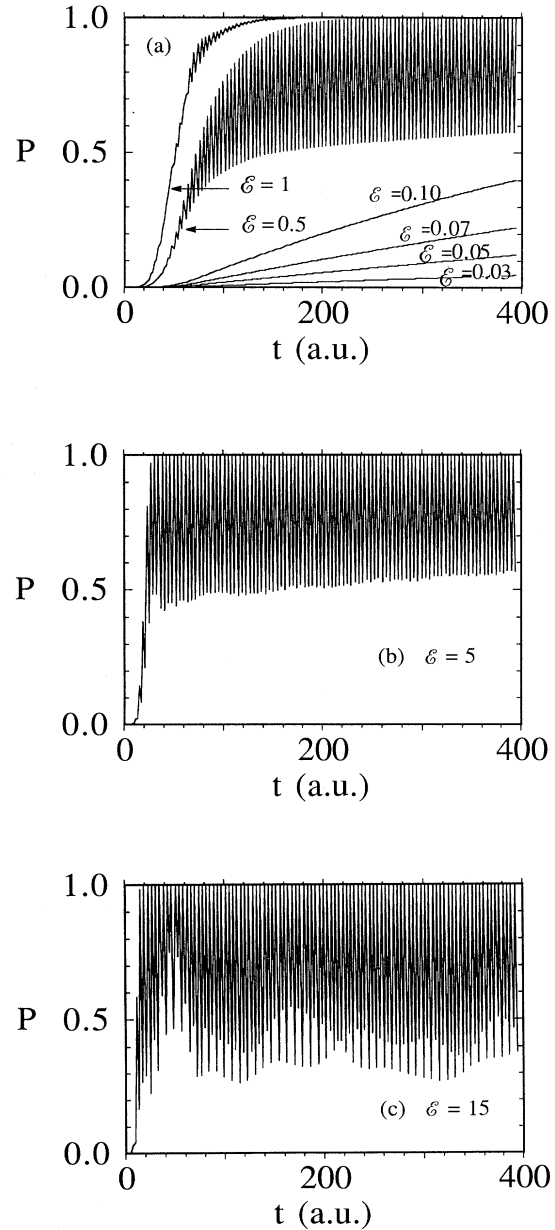

FIG. 2. Plots of the probability of ionization vs t for values of field strength from $\mathscr{E} = 0.03 - 15$. The wide oscillations evident every half-cycle for the case $\mathscr{E} = 0.5$ also occur for $\mathscr{E} = 1.0$, but we have shown only the maxima for graphical clarity.

bigger disagreements with the FGR prediction. For $\mathscr{E} = 0.05$, 0.07, and 0.10 the disagreements are 8.4%, 13%, and 23%, respectively, which shows that the lowest-order perturbative prediction is no longer very accurate as the intensities reach the order of 10^{14} W/cm^2.

We turn next to the strong-field region. It is important to stress that at the critical field strength, the potential structure changes to double-well from single-well form. In our plots (for $\omega = 0.8$) the field closest to the critical value is $\mathscr{E} = 1$. After the pulse turn-on ($t \geq 80.50$ a.u.) the population actually oscillates between 1 and about 0.5. We have plotted in Fig. 3 the population of bound levels labeled $n = 6$–20. Like the total positive-energy probability, the bound level population takes maximum values twice within each cycle but nearly vanishes between the maxima. The figure only shows the maxima clearly. As one could expect, the bound level populations vanish when the total positive-energy probability takes the value of unity. We believe the reason for the bound probability approaching zero twice within one cycle is that at specific times the electron is pushed far to one side ($x \sim \alpha_0 \sim 0.78$ in this case) and its associated wave function (wave packet) is almost orthogonal to the bound-state eigenfunctions of the field-free potential.

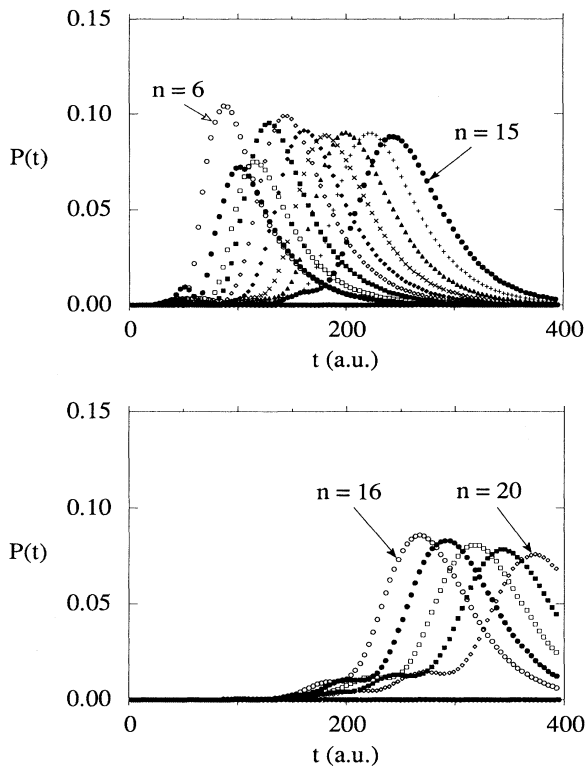When the field gets even stronger and enters the superstrong region we find in Figs. 2(b) and 2(c) that much of

the population is not permanently ionized. Within only 2–3 cycles (shorter than the turn-on time) the positive-energy population seems to be bounded by the values of 0.5 and 1. The rapid oscillation of this probability can be due to the same mechanism as in the strong-field cases. The localized wave function (wave packet) in the field-deformed potential moves back and forth with frequency ω and with amplitude α_0 ($\alpha_0 = 7.8$ and 23.4 for $\mathscr{E} = 5$ and 15, respectively). Therefore, twice in a cycle it is almost completely orthogonal to all the field-free bound states. The fact that the population is not really ionized but partly trapped will be further confirmed in the next section when we find that part of the probability remains near the origin throughout the laser pulse.

IV. PROBABILITY DENSITIES: TOTAL IONIZATION AND LOCALIZATION

In this section we study the electron's probability density $|\Psi(x,t)|^2$ as a function of its spatial variable x. We have already reported electron localization for two-photon ionization in a strong-laser field.[1] Here we will show that it can be observed in the one-photon case as well. Again our calculations suggest that electron localization relates closely to the potential deformation through the parameter α_0.

In Fig. 4 we have plotted the probability density versus position for six different field intensities. All of these plots are taken at 50 cycles after a 10.25 cycle of smooth pulse turn-on. Figure 4 clearly supports the intensity classification we introduced at the beginning of the last section. All the spatial plots presented here directly correspond to the ionization plots in Figs. 2(a)–2(c).

For $\mathscr{E} = 0.07$ and 0.10 in Fig. 4, most electrons can be

FIG. 3. Population on levels $n = 6$–20 during the excitation of a laser pulse with $\mathscr{E} = 0.5$ and 50.25 cycle duration and 10.25 cycle turn-on. These populations actually oscillate rapidly between 0 and the maxima evident in the plot.
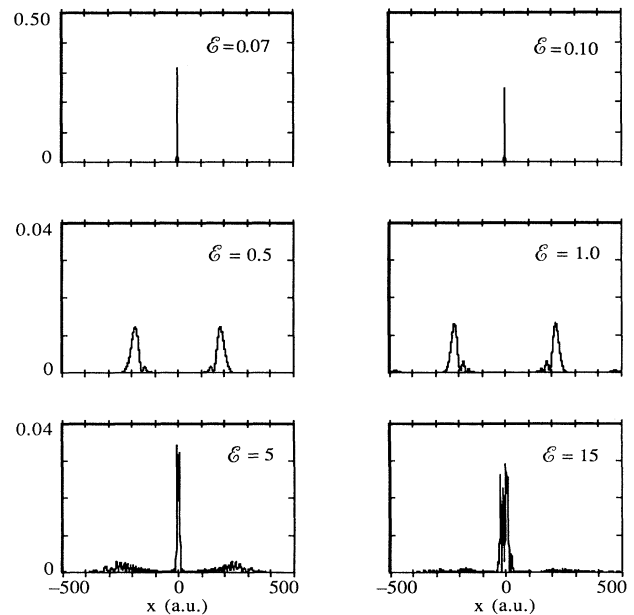
FIG. 4. Plots for various field strengths of the electron probability distribution at $t = 50$ cycles.

found close to the origin even at $t = 50c$. In these cases the total ionization is small, as indicated in Fig. 2(a). We can check from Fig. 1(b) that the bound levels are shifted only slightly. The ground state is only slightly depleted, so we expect that ionization may be described perturbatively.

The fields $\mathscr{E} = 0.5$ and 1.0 are strong but smaller than the critical field value so single-well ionization is still responsible for the process. As a result, we find in Fig. 4 that two wave packets are displaced from the center. To confirm that the electron cloud gradually drifts from the center of the potential, we have plotted in Fig. 5 snapshots of probability densities during the laser pulse for field strength $\mathscr{E} = 0.5$.

For the superstrong fields $\mathscr{E} = 5$ and 15 in Fig. 4, we find that a large part of the electron cloud remains near the origin while the rest moves away from the origin. We can also see roughly a two-peak structure for the part that is located near the origin. Measurements indicate that the separations of the peaks are about $2\alpha_0 = 15.6$ and 49.6. In addition to the separation of the central cloud, the cloud also oscillates around the origin at the optical frequency with an amplitude of α_0. These electron clouds are an imperfect version of the "dichotomy" found in the wave function calculations of the static field-deformed potential by Gavrila and co-workers.[4] The cycle average of these electron clouds generates three peaks located at $x = 0$, and $\pm\alpha_0$, which was predicted [4] for the hydrogen atom.

Notice that the "dichotomy" structure was not found for fields below the critical field strength (for $\mathscr{E} = 0.5$ and 1). Therefore the probability density plots confirm that the suppression of ionization or the electron localization in a field above the critical strength is due to the deformation of the potential well. These plots also indicate that ionization in a strong field is much more efficient than in a superstrong field. An increase of intensity over the critical value does not result in greater ionization but a more severe deformation of the potential, and part of the electron probability is stabilized near the atom.

V. ELECTRON ATI SPECTRA

In this section we will briefly mention the electron's kinetic-energy distribution above the threshold, which is conventionally called the ATI spectrum. This is the quantity $P(W,t) = |\langle W|\Psi(t)\rangle|^2$ plotted against the electron's kinetic energy W. As we have discussed in previous papers,[7-9] the ATI spectrum for a high-frequency laser with field intensity around 10^{13} W/cm^2 consists of a few distinct peaks separated by one photon energy. Weak-field ATI spectra are plotted on the first row in Fig. 6. Notice that ATI multiplets such as those reported previously[8] do not show up in one-photon ionization. As for strong and superstrong fields, plotted on the middle and the last row of Fig. 6, ATI peaks are harder to interpret. It appears that both plots in the same field group still look similar to each other, just as in Fig. 4. For strong fields, we can associate the wider ATI peaks with the drift velocity evident in Fig. 5.

We think it is interesting that the positions of the ATI peaks in each plot of Fig. 6 are closely predicted by the KH ground-state energy alone. Table I lists predicted ATI peak positions as well as the observed positions for different field strengths. The numbers on the first row represent weak-field values since they are virtually the same, to the displayed accuracy. The predicted first ATI peak positions are calculated with the following formula (note the absence of a term for a "pondermotive" threshold shift):

$$E^{(ATI)}_{predicted} = W_g(\mathscr{E}) + \hbar\omega , \qquad (13)$$

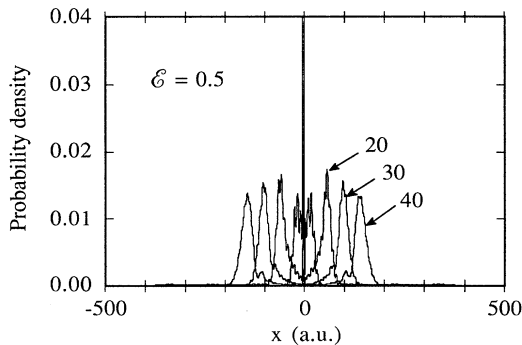where $W_g(\mathscr{E})$ represents the ground-state energy in the

FIG. 5. Electron probability distribution at various times, showing prompt drift of the electron away from the origin in the case of the subcritical field strength $\mathscr{E} = 0.5$. The labels on the curves give the time t increased by $0.25c$ for ease of reading (i.e., 20 means $19.75c$, etc.).
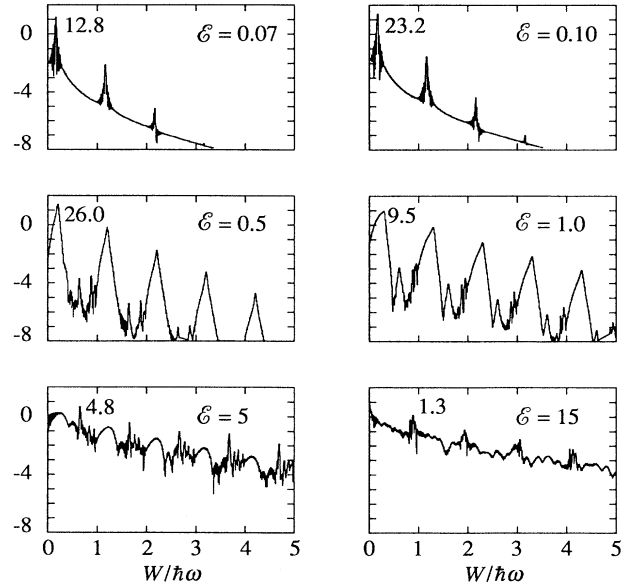

FIG. 6. Plots for various field strengths of the electron above-threshold probability distribution against its kinetic energy. The number on the upper-left corner of each plot gives the height of the first ATI peak.

TABLE I. The lowest ATI peak positions predicted by Eq. (13) and those measured from the plots in Fig. 6. The value of the ground level in the average KH frame, displayed in Fig. 1(b), is also listed for various field strengths. The last three columns are measured in units of the photon energy.

$\mathcal{E}$	$W_g(\mathcal{E})$	$E^{(ATI)}_{predicted}$	$E^{(ATI)}_{observed}$
0.0	-0.838	0.162	0.162
0.5	-0.800	0.200	0.204
1.0	-0.720	0.280	0.290
5.0	-0.364	0.646	0.653
15.0	-0.184	0.816	0.885

field-deformed KH potential and $\hbar\omega$ is the photon energy. All quantities in the last three columns in Table I are measured in units of the photon energy. The agreement between the predicted and the observed values is quite good up to $\mathcal{E}=5$ at least. We must mention that an estimate based on the ac Stark shift of the ground state and the usual pondermotive threshold shift does not give such a good agreement for any of the strong- or superstrong-field cases.

VI. SUMMARY

We have demonstrated in this paper that one-photon ionization of a one-dimensional one-electron atom occurs in three different ways. For weak-field cases, the ionization follows reasonably closely the predictions of perturbation theory. For strong fields, the atom will be quickly totally ionized. For superstrong fields, the ionization becomes much less efficient. Ionization suppression can be easily understood if we take into account that a super-

strong field very severely deforms the atomic binding potential. If this potential deformation takes place before the atom is totally ionized, then the deformed potential will localize the electron and prevent its further ionization.

We have previously reported our calculations[1] for a two-photon ionization process. In both one- and two-photon ionizations, the suppression of ionization has been found for superstrong fields. We agree with the earlier emphasis by Gavrila and co-workers,[4] that the parameter controlling high-frequency ionization is $\alpha_0 = \mathcal{E}/\omega^2$ rather than directly $\mathcal{E}$ or ω. In contrast to earlier predictions,[3,4] we have found that the frequency ω need not be asymptotically large.

We have confirmed that in ionization by intense laser fields one can easily predict various effects by adopting the KH frame. The application of this frame does have limitations; ideally it only works for lasers with infinitely high frequency. If our conclusions can be extended to three-dimensional situations (not at all certain) and to appropriately scaled ground-state energies (recall Ref. 10), it might be possible to use very short-pulse short-wavelength lasers, such as excimer or frequency-doubled dye lasers, to see ionization suppression at intensities around 10^{16} W/cm^2 and much more efficient ionization below this value.

ACKNOWLEDGMENTS

[1]For previous work along these lines, see Q. Su, J. H. Eberly, and J. Javanainen, Phys. Rev. Lett. **64**, 862 (1990); Q. Su and J. H. Eberly, J. Opt. Soc. Am. B **7**, 564 (1990); J. H. Eberly and Q. Su, in *Proceedings of the X Vavilov Conference,* edited by S. G. Rautian (Nova, New York, 1990).

[2]W. C. Henneberger, Phys. Rev. Lett. **21**, 838 (1968); F. H. M. Faisal, J. Phys. B **5**, L89 (1973).

[3]J. I Gersten and M. H. Mittleman, J. Phys. B **9**, 2561 (1976).

[4]M. Gavrila and J. Kaminski, Phys. Rev. Lett. **52**, 613 (1984); M. Pont, N. R. Walet, M. Gavrila, and C. W. McCurdy, *ibid.* **61**, 939 (1988); M. Pont, N. R. Walet, and M. Gavrila, Phys. Rev. A **41**, 477 (1990).

[5]H. A. Kramers, *Collected Scientific Papers* (North-Holland, Amsterdam, 1956).

[6]J. H. Eberly and J. Javanainen, Eur. J. Phys. **9**, 265 (1988).

[7]J. Javanainen, J. H. Eberly, and Q. Su, Phys. Rev. A **38**, 3430 (1988); J. Javanainen and J. H. Eberly, J. Phys. B **21**, L93 (1988).

[8]J. H. Eberly and J. Javanainen, Phys. Rev. Lett. **60**, 1346 (1988).

[9]J. H. Eberly, Q. Su, and J. Javanainen, Phys. Rev.Lett. **62**, 881 (1989).

[10]J. H. Eberly, Phys. Rev. A **42**, 5750 (1990).